A fully probabilistic framework to compute the residual rockfall risk in presence of mitigation measures

Technical Note

Landslides
DOI 10.1007/s10346-024-02377-8
Received: 3 February 2024
Accepted: 25 September 2024

Maddalena Marchelli · Valerio De Biagi · Bernardino Chiaia

A fully probabilistic framework to compute the residual rockfall risk in presence of mitigation measures

Abstract Rockfall events are expected to rise throughout the future due to climate change and extreme meteorological events. In the perspective of climate change adaptation, an accurate quantification of the risk is needed, together with a precise assessment of the effectiveness of protective measures eventually installed. All the possible block detachment scenarios together with their occurrence probability should be considered, and a time span should be selected. A fully probabilistic framework to compute the risk in absence and in presence of a protective structure is herein proposed, and a time-integrated reliability-based method, developed by the authors, is applied to define the failure probability of the protective measure. The complete method, in absence and presence of a rockfall barrier, is applied to a study case, and the residual risk in presence of the barrier is quantified. The results show the importance of considering all the possible detachment situations to have reliable results in terms of both risk and effectiveness of the protective measure quantification.

Keywords Quantitative risk assessment · Residual rockfall risk · Probabilistic assessment · Protective measure

Introduction

Climate change and the occurrence of extreme events are becoming crucial in the next future. Permafrost and rock degradation and massive glaciers retreat by global warming effects of climate change have a direct impact on mountain areas (Knoflach et al. 2021; Allen and Huggel 2013), and recent studies have highlighted a significant increase of the frequency of rockfall phenomena (Ravanel and Deline 2015; Hartmeyer et al. 2020; Mirhadi and Macciotta 2023). As an example, Stoffel et al. (2024), analyzing a continuous time series from 1920 to 2020 of periglacial rockfall activity at Täschgufer (Swiss Alps), have shown as the ongoing warming favors the release of rockfall. Although the scientific community recognizes a well-established link between climate change and rockfall at the high altitudes, the correlation in middle mountain and low elevations is still under debate (Jakob 2022; D'Amato et al. 2016; Mainieri et al. 2023). Nevertheless, the growing number of people (Langenbach and Jaccard 2019) and infrastructures in mountain regions increment the vulnerability and exposure (Gasser 2022) and, thus, the potential risk. To deal with such phenomena, adaptation strategies must be implemented (SDG 13, DESA 2023), underlining the urgency for both an accurate rockfall risk assessment and effective risk mitigation strategies.

A quantification of the risk is often required by authorities to manage and quantify the effectiveness of mitigation plans, meaning that accurate hazard and consequences analyses have to be performed (Corominas et al. 2014; Marchelli et al. 2022). The analysis starts from the identification and characterization of the possible initiating events, defining all the possible release scenarios from which propagation analyses are performed. Each scenario is characterized by an occurrence frequency and several characteristics of the block involved in the phenomenon (e.g., size, initial velocity, shape, orientation) (Wang et al. 2014; De Biagi et al. 2017; Moos et al. 2022). Propagation analyses account for the variability of the rock and soil characteristics and interaction parameters, the slope topography, and the quality of the propagation model (Scavia et al. 2020). Neglecting empirical propagation models, i.e., focusing on trajectory models, the simplest approach is the 2D lumped mass analysis. More accurate modeling considers all the possible types of motion of the block according to its characteristics (Li and Lan 2015). To deal with such an amount of variables and outcomes, probabilistic approaches are required (Lari et al. 2014; Macciotta et al. 2015; Rossi et al 2021). As a result, the hazard, which is the probability that an event of a given intensity occurs in a given time and in a given space, can be computed.

For each starting event and its evolution, the consequences have to be assessed to obtain the risk value for a given element in a given time period (Crosta et al. 2015). As the hazard, the consequences must account for all the possible released volumes that can be generated by the rock face, together with their frequency (Farvacque et al. 2021). The effects can be quantified as the product between vulnerability, which is the degree of loss subsequent to the event, and the value. Combining hazard, consequences and exposure, the risk is computed. In general, the risk for a single scenario can be mathematically described as (Corominas et al. 2014; Hantz et al. 2021)

$$R = \left[P\left(V_i\right)P\left(X_j|V_i\right)\right]E\left(T|X_j\right)V\left(V_i,X_j\right)W \quad (1)$$

where R is the risk, P is the probability associated to the release of a block of size V_i, $f_2\left(X_j|V_i\right)$ is the probability that the block of size V_i reaches the point X with an intensity j, $E\left(T|X_j\right)$ is the exposure, i.e., the probability that the element is along the trajectory of the block at the point X when the rockfall occurs, i.e. at time T, and $V\left(V_i,X_j\right)$ is the vulnerability, i.e., the degree of loss of a given element at risk considering the block of size V_i and the intensity j. The term W refers to the value of the element, i.e., the degree of importance, quantified in monetary terms, for direct or indirect costs, or with a graded scale. Depending on the type of the elements, losses and values can be considered from a physical, economical, social, or environmental point of view (Amatruda et al. 2004). It must be noted that all the terms except W are dimensionless in the range [0;1]. Only W has a unit. The terms into the square brackets are

commonly referred to the hazard $H(V_i, X_j)$. To account for multiple scenarios, e.g., when different blocks sizes can be released with different release frequencies, the common practice is to either (i) consider the worst scenario, only, or (ii) sum the single risks approximating $P(V_i)$ with the frequency of occurrence of each block size. Both approaches approximate the true risk: the former does not consider the effects of smaller, but more frequent, rockfalls, the latter not accurate results if rockfalls are frequent.

When the risk value is higher than an acceptable threshold, mitigation measures have to be adopted. Among structural mitigation measures, and particularly among protective ones, net fences (i.e., flexible rockfall barriers) or embankments are about the most effective for high energy events (Peila and Ronco 2009; Vigna et al. 2023). In the current practice, the protective measure is designed with respect to a given scenario, intended as a released block size (Vagnon et al. 2020; UNI 11211-4 2018; ONR 24810 2021). Its failure probability, computed by considering the distribution of energy and trajectory height, does not encompass the inherent variability of the released blocks and their occurrence. As a result, the quantified effectiveness of the protective measure is related to a single scenario, outside a specific time framework. Climate change modifies the rockfall activity of the face, increasing the number of events per interval time (Macciotta et al. 2017). The single-scenario analysis is, thus, incompatible with the needs of adaptation fostered by SDG 13.

Recently, the authors proposed a time-integrated reliability-based design approach (De Biagi et al. 2020; Marchelli et al. 2020, 2021), where the reliability calculation accounts for the variability in magnitude of the events, their occurrence probability, and for the intrinsic variability of the actions, with non-fixed probability distributions. It has to be noted that, although the risk mitigation measures are installed to protect the element, the residual risk is not null as the protection measure has an intrinsic failure probability. The effectiveness of the protective measure can be quantified through the residual risk which must be computed by time-integration of all the possible release scenario that can happen. In this case, the increasing frequency of the events due to climate change can be considered.

To this aim, the present paper details a fully probabilistic framework to compute the risk in absence and in presence of a protective structure. The methodology is described in Section "Methodology." For the sake of simplicity, for the calculations related to the failure of the protective measure, references to previous papers by the authors are provided. In Section "Study case and application," an example of application is proposed, stressing which assumptions can be done. Conclusions follow in the last section.

Methodology

Rockfall risk on a given element located on the slope depends on several factors: the released volume and its occurrence frequency, the possibility that the volume fragments during the propagation, the possibility that the block reaches the element, the kinematic properties of the falling volume at the location of the element, the vulnerability and the exposure, and the presence of passive protective measures (say rockfall barriers or rockfall embankments). Active protective measures affect the occurrence frequency of the phenomenon. The observations on real rock faces show that smaller volumes are more likely to detach than larger blocks. Previous studies on in-situ block size distributions (IBSD) highlight that the discontinuity patterns of the rock mass identify potentially unstable rock blocks which volumes can be described through an exponential-like distribution (Ruiz-Carulla et al. 2017; Illeditsch and Preh 2024). Anyway, the detachment process is affected by several factors; hence, it is possible that the distribution of the detached volumes does not follow the IBSD. We call as f_1 the probability density function of the released volumes, i.e., the function that describes the size of the falling rock block volume, when released. Similarly to De Biagi et al. (2017), the process of the occurrences can be described as a Poisson point process (Crovelli 2000; McClung 1999) with a mean annual frequency of block detachment of any size equal to $\lambda^\star$ and differs from the definition of the falling volumes. Hence, f_1 does not contain the temporal information, and it can be defined as the probability distribution of the released rock block volume, $V^\star$, when a release occurs.

Under the hypothesis that fragmentation during propagation does not occurs, for a given slope with different soil properties, the type of motion of the released mass is affected, among other factors, by its volume. It results that just a fraction of the released volumes, known as reach probability, can reach the location at which the element at risk is located. In the present framework, the reach probability, f_2, for a given slope (characterized by topography, soil conditions, etc.) is a function of the released volume, i.e., $f_2(V^\star)$. If a lumped mass model is used for propagation analyses, the reach probability f_2 has a constant value and the average rate of occurrence of rockfall blocks at the location of the element at risk is equal to $f_2\lambda^\star$, and the distribution of the blocks at the slope toe is identical to f_1.

In a given point of the slope, the distribution of the velocities, v, depends on the size, V, of the released block. In general, the probability density function of the velocity, f_v, can be written as $f_v(v, V = V^\star)$. The vulnerability of a possible impacted element depends on the characteristics of the element and the intensity of the phenomenon. For rockfalls, the intensity is expressed as the kinetic energy of the falling rock. Hence, the vulnerability of a given element, Φ, is a function of the velocity, v, and the volume, $V^\star$, i.e., $\Phi(v, V^\star)$. The exposure, E, on the contrary, does not depend on the phenomenon itself.

Risk quantification in case of absence of any protection measure

For a given falling block occurrence scenario, i.e., the detachment of a given volume that arrives at the element at risk, the vulnerabilities with respect to all the possible velocities that the block can have must be computed. It results that the risk can be expressed as

$$R = E \iint_0^\infty \left[1 - e^{-\lambda^\star f_1(\mu) f_2^e(\mu)\tau}\right] V(\psi, \mu) f_v(\psi, V = \mu) d\psi\, d\mu, \qquad (2)$$

where $f_v(\psi, V = \mu)$ is the probability density function of the velocity (ψ) considering the released block size μ and $f_2^e(\mu)$ is the reach probability at the element at risk. The term into the square brackets represents the probability of occurrence (during the time period τ) of the specific scenario of the arrival of a block with volume equal to μ. It derives from Poisson probability mass function considering the occurrence of at least one event. If the term $-\lambda^\star f_1(\mu) f_2^e(\mu)\tau$ is close to zero, thanks to McLaurin series, the square bracket can be approximated into

$$1 - e^{-\lambda^\star f_1(\mu) f_2^e(\mu)\tau} \approx \lambda^\star f_1(\mu) f_2^e(\mu)\tau, \tag{3}$$

and Eq. 2 becomes

$$R = E \iint_0^\infty \left[\lambda^\star f_1(\mu) f_2^e(\mu)\tau\right] V(\psi,\mu) f_v(\psi, V=\mu) d\psi d\mu. \tag{4}$$

In case the vulnerability has a value that does not depend on the intensity of the phenomenon, hence it can be considered constant, Eq. 2 turns into

$$R = E\, V \int_0^\infty \left[1 - e^{-\lambda^\star f_1(\mu) f_2^e(\mu)\tau}\right] d\mu. \tag{5}$$

In addition, if a lumped mass propagation model is adopted, as stated, f_2^e is equal for each block size. Noting that $\int_0^\infty f_1 d\mu = 1$, Eq. 5 can be further simplified into

$$R = E\, V \left[1 - e^{-\lambda^\star f_2^e \tau}\right]. \tag{6}$$

If the simplification reported in Eq. 4 holds, Eq. 6 can be written as

$$R = \left[\lambda^\star f_2^e \tau\right]\, V\, E, \tag{7}$$

where the term into square brackets represents the hazard.

Risk quantification in presence of a protective measure

In case a protective measure is installed along the slope, the potential hazardous scenario derives from the failure of the measure due to a given falling block occurrence. Given that the protective measure has n independent failure scenarios, it results

$$R = E \iint_0^\infty \sum_{i=1}^{n} \left\{ \left[1 - e^{-\lambda^\star f_1(\mu) f_2^p(\mu) A_i(\mu)\tau}\right] \Phi_i(\mu) V(\psi,\mu) \tilde{f}_{v,i}(\psi, V=\mu) \right\} d\psi d\mu, \tag{8}$$

where $A_i(\mu)$ is the failure probability associated to the ith failure mode of the protective measure when the arrival of a detached block of size μ occurs, and f_2^p is the reach probability at the location of the protective measure. The term $\Phi_i(\mu)$ serves to consider that a fraction of the blocks arriving and passing the barrier (as their energy or trajectory height are larger than the capacity of the system) cannot reach the element at risk. It must be smaller than one, and it is thus expressed as

$$\Phi_i = (\mu) \min \left[\frac{\tilde{f}_{2,i}^e(\mu)}{f_2^p(\mu)}; 1\right]. \tag{9}$$

The terms $\tilde{f}_{2,i}^e(\mu)$ and $\tilde{f}_{v,i}(\psi, V=\mu)$, referred to the element at risk, are modified with respect to Eq. 2 to account that the protective measure, damaged according to the ith failure mode, might change the reach probability and the velocities of the blocks that eventually arrive at the element at risk.

For rockfall barriers, as proposed by several scholars and by the authors (Marchelli et al. 2021), the number of failure modes is equal to two: one failure ($i = 1$) is associated to the excessive kinetic energy, and the other ($i = 2$) to the excessive trajectory height. In case of failure associated to a kinetic energy that is greater than barrier energy absorption capacity ($i = 1$), it results

$$A_1(\mu) = \iiint_0^\infty p_{f,k}\left(V=\mu, v_{95}=\omega, r=\rho\right) f_{v_{95}}(\omega, V=\mu) f_{v_{99}}(\nu, V=\mu) f_r\left(\rho, v_{95}=\omega, v_{99}=\nu, V=\mu\right) d\omega d\nu d\rho, \tag{10}$$

where $p_{f,k}\left(V=\mu, v_{95}=\omega, r=\rho\right)$ is the failure probability of the barrier due to kinetic energy considering that the block size has a mean size equal to μ, the distribution of the velocity has a 95th percentile equal to ω, and the ratio between 99th and 95th percentiles is equal to ρ. $f_{v_{95}}(\omega, V=\mu)$ and $f_{v_{99}}(\nu, V=\mu)$ are the probability density functions of the 95th and 99th percentiles, respectively, of the velocity for a given block size μ. The $f_r\left(\rho, v_{95}=\omega, v_{99}=\nu, V=\mu\right)$ is the joint probability density function of the ratio between the 99th and the 95th percentiles of the velocity. Figure 1 depicts the probability density functions of $f_{v_{95}}$ and $f_{v_{99}}$ for two values of μ.

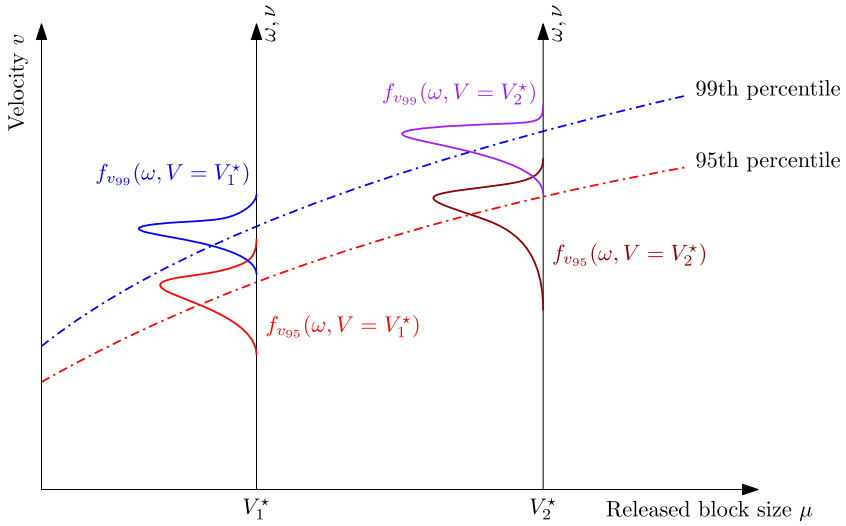

Fig. 1 Probability density functions of $f_{v_{95}}$ and $f_{v_{99}}$ for $\mu = V_1^\star$ and $V_2^\star$. The thick dotted lines represent the means (50-percentile) of the distributions

Fig. 2 View of the source area (left) and the deposit (right) where the elements at risk are located

The probability density functions $f_{v_{95}}$, $f_{v_{99}}$, and f_r serve to account for the uncertainties related to the selection of the propagation model. In the majority of the cases, the probability density functions can be substituted with Dirac-δ distributions located at the values of $v_{95}(V=\mu)$, $v_{99}(V=\mu)$, and $r=v_{99}/v_{95}$, and Eq. 10 can be rewritten as

$$A_1(\mu) = p_{f,k}\left(V=\mu, v_{95}, r\right). \tag{11}$$

In case of failure associated to block trajectory height greater than barrier height ($i=2$), it results

$$A_2(\mu) = \iiint_0^{\infty} p_{f,h}\left(V=\mu, h_{95}=\theta, p=\pi\right) f_{h_{95}}(\theta, V=\mu) f_{h_{99}}(\eta, V=\mu) f_p\left(\pi, h_{95}=\theta, h_{99}=\eta, V=\mu\right) d\theta d\eta d\pi, \tag{12}$$

where $p_{f,h}\left(V=\mu, h_{95}=\theta, p=\pi\right)$ is the failure probability of the barrier due to the height considering that the block size has a mean size equal to μ, the distribution of trajectory height has a 95th percentile equal to θ, and the ratio between 99th to 95th percentiles is equal to π. $f_{h_{95}}(\theta, V=\mu)$ and $f_{h_{99}}(\eta, V=\mu)$ are the probability density functions of the 95th and 99th percentiles, respectively, of the velocity for a given block size μ. The $f_p\left(\pi, h_{95}=\theta, h_{99}=\eta, V=\mu\right)$ is the joint probability density function of the ratio between the 99th and the 95th percentiles of the height. Similarly as before, the probability density functions $f_{h_{95}}$, $f_{h_{99}}$, and f_p serve to account for the uncertainties related to the selection of the propagation model. In the majority of the cases, the probability density functions can be substituted with Dirac-δ distributions located at the values of $h_{95}(V=\mu)$, $h_{99}(V=\mu)$, and $p=h_{99}/h_{95}$, and Eq. 12 can be rewritten as

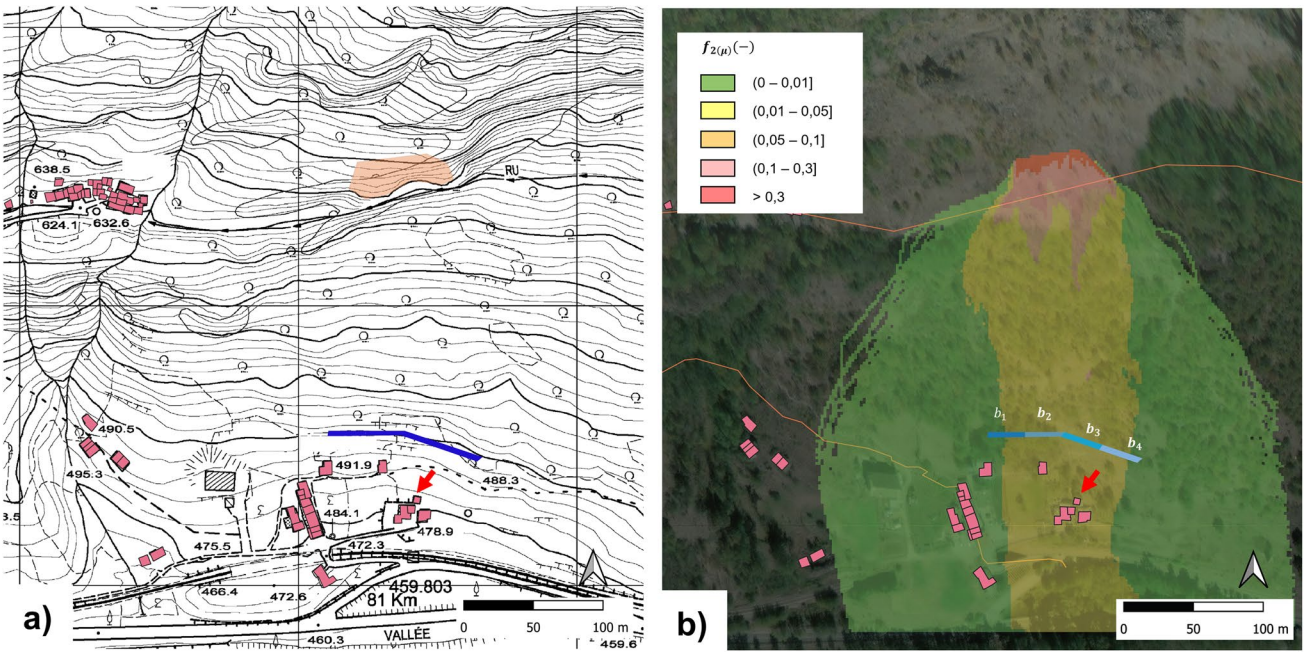

Fig. 3 Study case: **a** identification of the source area (orange), barrier location (blue line), and of the element at risk (red arrow); **b** reach probability $f_2(\mu)$. The case of $V^\star = 5\text{m}^3$ is considered

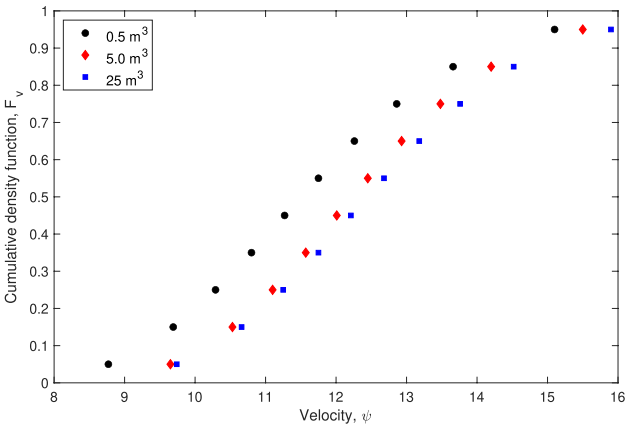

Fig. 4 Velocity distribution at the element at risk evaluated as a LN distribution starting from 95th and 99th percentiles

$$A_2(\mu) = p_{f,h}\left(V = \mu, h_{95}, p\right). \tag{13}$$

Study case and application

The aforementioned methodology was applied to a study case in Aosta Valley, in the Northwestern Italian Alps (Fig. 3a). The study area exhibits a distinct geological and structural context characterized by rocks from the Piedmontese Calcescist Zone. These rocks include green stones covered by quartzites, marbles, and mycascists, forming two primary groups of ophiolitic units. The predominant outcrops in the examined region belong to the Zermatt-Saas eclogitic units, comprising dominant ophiolites and metasedimentary covers. Eclogitic relicts are widespread, and a metamorphic overprint in green schist facies is evident, ranging from incipient to complete. Notably, extensive sequences of ophicalci, visible in quarries, suggest potential tectonic denudation processes of the mantle.

From a structural perspective, the valley aligns in an East–West direction, situated along an Oligogenic Age tectonic depression. The primary fault, running E-W, forms a tectonic system approximately 2 km wide, shaping an asymmetrical graben. A detailed topographic survey, conducted through photogrammetric helicopter surveys, aimed to investigate and characterize the area. Laser scanners, positioned on the opposite valley side, were utilized to discern and characterize the rock mass while minimizing shadow zones and reducing disturbance to the abundant vegetation on the slopes.

Table 2 Calculations of the failure properties of the barrier

	$V^\star$ (m^3)	f_2^p (-)	v_{95} (m/s)	v_{99} (m/s)	$A(\mu_i)$ (-)
b_1	0.5	0.012	16.2	16.9	0.00E+00
	5.0	0.012	16.6	18.0	1.20E-09
	25	0.013	16.7	18.4	5.66E-01
b_2	0.5	0.035	18.3	19.3	0.00E+00
	5.0	0.030	18.3	20.0	1.23E-06
	25	0.028	18.4	20.5	6.44E-01
b_3	0.5	0.040	19.1	20.9	0.00E+00
	5.0	0.030	19.2	21.0	1.00E-05
	25	0.030	19.4	21.1	8.88E-01
b_4	0.5	0.020	16.3	17.3	0.00E+00
	5.0	0.015	16.8	18.1	4.50E-10
	25	0.015	17.0	18.7	6.11E-01

The reliability-based approach proposed by the authors was adopted. The calculations are replicated for the four parts into which the 120 m long barrier was divided

Processed and elaborated data were employed to delineate potential source areas for detachment, identifying the most fractured zones, past event source zones, and unstable blocks. Despite the diverse geological units on the slope under examination, all sectors share common systems of discontinuity. The primary discontinuity systems, though varying in representation based on outcrop orientation, were consistent across the study area. Kinematic analyses identified potential instability mechanisms, revealing a uniform trend in all sectors. This uniformity stemmed from similarities in geomechanical properties (friction angle), structural aspects (discontinuity family locations), and morphometric features (slope locations) within the investigated area. Zones exhibiting heightened fracturing, with observed sliding and toppling mechanisms, were pinpointed for further scrutiny.

Figure 2 depicts an aerial view of the source area and the deposit, where several buildings are located. As an example of application, the risk is computed for the building in the red square.

As a static element, the exposure E of the building is unitary. In the present analysis, the value is not considered. Hence, the risk is

Table 1 Risk on the construction in case no protective measures are installed

$V^\star$ (m^3)	$F_1(\mu_i)$ (-)	f_2^e (-)	v_{95} (m/s)	v_{99} (m/s)	$\sum_{j=1}^{M}\left[V(\psi_j,\mu_i)f_v(\psi_j,V=\mu_i)\Delta\psi_j\right]$ (-)	$R(\mu_i)$ (yr^{-1})
0.5	0.900	0.030	15.1	16.9	0.223	6.02E-04
5.0	0.098	0.029	15.5	17.1	0.996	2.83E-04
25	0.002	0.027	15.9	17.6	1.000	5.40E-06
R						8.90E-04

The last row refers to the summation over the i-indices related to the size of the detached block

Table 3 Risk analysis calculations on the element at risk when a 120 m 5000 kJ rockfall barrier is present

	$V^\star$ (m^3)	f_2^p (-)	$\tilde{f}_2^e$ (m/s)	Φ (-)	$A(\mu_i)$ (-)	$R(\mu_i)$ (yr^{-1})
b_1	0.5	0.012	0.030	1.000	0.00E+00	0.00E+00
	5.0	0.012	0.029	1.000	1.20E-09	1.41E-13
	25	0.013	0.027	1.000	5.66E-01	1.47E-05
R						1.47E-05
b_2	0.5	0.035	0.030	0.857	0.00E+00	0.00E+00
	5.0	0.030	0.029	0.967	1.23E-06	3.48E-10
	25	0.028	0.027	0.964	6.44E-01	3.48E-05
R						3.48E-05
b_3	0.5	0.040	0.030	0.750	0.00E+00	0.00E+00
	5.0	0.030	0.029	0.967	1.00E-05	2.83E-09
	25	0.030	0.027	0.900	8.88E-01	4.80E-05
R						**4.80E-05**
b_4	0.5	0.020	0.030	1.000	0.00E+00	0.00E+00
	5.0	0.015	0.029	1.000	4.50E-10	6.59E-14
	25	0.015	0.027	1.000	6.11E-01	1.83E-05
R						1.83E-05

The worst condition is highlighted by bolted numbers

expressed as a damage probability. The contribution of a 120 m long, 7 m high, 5000 kJ barrier located upwards the building to mitigate the risk is evaluated by comparing the risks without and with the barrier. The procedure illustrated in Sect. "Methodology" is applied.

The studies in the area shown that the block sizes that can be released from the cliff face can be binned into three main size categories: 0.5, 5, and 25 m^3. The average release frequency, as monitored from onsite survey, is 1 event every 10 years, hence $\lambda^\star = 0.1\,\mathrm{yr}^{-1}$. Blocks belonging to 0.5 m^3 are more likely to release, while larger blocks are more rare. To keep the procedure easier to understand, the proposed integral formulation of Eqs. 2 and 8 is rewritten in finite sums thanks to the summation operator. The risk without any protective measure, i.e., Eq. 2, can be rewritten as

$$R = \sum_{i=1}^{N} \left\{ \left[1 - e^{-\lambda^\star F_1(\mu_i) f_2^e(\mu_i) \tau} \right] \sum_{j=1}^{M} \left[V(\psi_j, \mu_i) f_v(\psi_j, V = \mu_i) \Delta\psi_j \right] \right\}. \tag{14}$$

Summation index i describes the release volumes, and the summation index j describes the values of block velocities at the location of the element at risk. The term $F_1(\mu_i)$ is the integral of f_1 among the bounds defined by the bins of each volume class. Table 1 details, in the second column, the values of $F_1(\mu_i)$ for the three volume classes. It means that, among the released blocks, those belonging to 5 m^3 class are the 9.8%.

Trajectory analysis was performed with the 3D code Rockyfor3D (Dorren 2015), which implements a hybrid propagation model, mass-dependent. A digital elevation model with a grid 2 × 2 m was used, considering 100 runs per cell of the source zone as a statistically representative sample of simulations. The reach probability $f_2(\mu)$ was defined for all the investigated scenarios. The barrier was subdivided in 4 parts of equal length, $b_1 - b_4$, and, for each, the mean values of $f_2^b(\mu)$, v_{95}, and v_{99} are assumed representative of the whole part (Fig. 3b).

Block velocities ψ at the location of the element at risk are evaluated by supposing that the square of the velocities follows a lognormal (LN) distribution (Agliardi et al. 2009; Spadari et al. 2013). To make the summation, the entire domain of the LN distribution has been divided into non-homogeneous 10 parts in such a way that the values correspond to the 5th, 15th, up to the 95th percentiles of the distribution, as shown in Fig. 4. It results that the product $f_v(\psi_j, V = \mu_i)\Delta\psi_j$ is equal to 0.1.

Once the values of the velocity are determined, the vulnerability of the element at risk, a construction, is computed. The general formula provided by Agliardi et al. (2009) was considered:

$$V(\mu_i, \psi_j) = 1 - \frac{1.358}{1 + \exp\left(\frac{1350\mu_i\psi_j^2 - 129000}{120300} \right)} \tag{15}$$

The risk is computed thanks to the summation reported in Eq. 14. As the interest is on the annual risk, τ was set to 1 (year). Table 1 summarizes the results. The total yearly risk is equal to 9.40×10^{-4}.

The presence of a protective measure modifies the risk on the construction. The 120 m long barrier was divided into 4 parts. As the barrier is a series-like system, it was assumed that the barrier fails if one of its modules fails. The failure of the

barrier associated to a specific velocity and falling volume was computed thanks to the reliability formulae proposed by the authors in previous papers (De Biagi et al. 2020; Marchelli et al. 2021, 2022). For the sake of clarity, the details on the calculations are not here reported as can be found by computing the Hasofer-Lind transformation of the variables. In the reliability calculations, it is assumed that the coefficient of variation of the falling mass is 0.1 and the capacity of the barrier has a Dirac-δ distribution at 5000 kJ. Table 2 details the calculations of the failure of the barrier for each of the four parts. The failure term, $A(\mu_i)$, is reported in column six.

The risk on the construction was computed considering that the barrier does not modify the reach probability computed without the protective structure; hence, the $\tilde{f}_2^e$ is equal to the one reported in Table 1. It is also assumed in the present example that the barrier does not modify the distribution of the velocities at the location of the element at risk. Hence, the cumulative density function of the velocity is the one reported in Fig. 4. Table 3 details the calculation on the vulnerability on the building and the final risk when the protective structure is present. The worst case is associated to the failure of a module in b_3: the resulting risk on the construction is 4.80×10^{-5}. The protective structure mitigates the risk of about two orders of magnitude, roughly.

Conclusions

The present paper addresses the problem of the calculation of rockfall risk in mountain slope. The proposed approach consists in a time-integrated procedure that accounts for all the possible release volumes that can detach, together with their probability. Differently from the commonly used approaches, all the scenarios are considered and weighted to obtain the total risk. The time-integrated approach allows to measure the risk for a given temporal range, say 1 year.

The method allows to include a protective structure, whose effectiveness can be computed through a reliability-based methodology. Comparing the risks without and with the protective structure, the residual risk and the effectiveness of the mitigation measure can be quantified in a specific time framework.

The proposed method to quantify the risk takes advantage of the continuous functions that describe the properties and characteristics of the natural phenomenon. Meanwhile, the authors have proposed a discrete formulation that well fits when the knowledge on the phenomenon is limited, e.g., when the size of the released blocks fits within a specific range (binned situation).

The comparison between protected and unprotected scenarios highlights interesting considerations: the protective structure has a failure probability; hence, the presence of the barrier reduces the risk, but it does not set it to zero, null risk.

Including fragmentation during rockfall propagation is expected to provide a more realistic evolution of the detachment of a block, with consequences on the risk in the inhabited mountain areas.

Funding

This study was carried out within the RETURN Extended Partnership and received funding from the European Union Next-GenerationEU (National Recovery and Resilience Plan – NRRP, Mission 4, Component 2, Investment 1.3 – D.D. 1243 2/8/2022, PE0000005) – SPOKE TS 2 and within the Marie Curie Postdoctoral Fellowship 2022 (Call Horizon-MSCA-2022-PF-01, Grant GA101103401, RIDETHERISK project).

Data Availability

The data that support the findings of this study are available from the corresponding author upon reasonable request.

Declarations

Conflict of interest The authors declare that they have no known competing financial interests or personal relationships that could have appeared to influence the work reported in this paper.

References

Agliardi F, Crosta G, Frattini P (2009) Integrating rockfall risk assessment and countermeasure design by 3D modelling techniques. Nat Hazards Earth Syst Sci 9(4):1059–1073

Allen S, Huggel C (2013) Extremely warm temperatures as a potential cause of recent high mountain rockfall. Glob Planet Chang 107:59–69

Amatruda G, Bonnard C, Castelli M et al (2004) A key approach: the IMIRILAND project method. In: Identification and mitigation of large landslide risks in Europe. CRC Press, p 31–62

Corominas J, van Westen C, Frattini P et al (2014) Recommendations for the quantitative analysis of landslide risk. Bull Eng Geol Environ 73:209–263

Crosta GB, Agliardi F, Frattini P et al (2015) Key issues in rock fall modeling, hazard and risk assessment for rockfall protection. In: Engineering geology for society and territory-volume 2: landslide processes, Springer, pp 43–58

Crovelli RA (2000) Probability models for estimation of number and costs of landslides. Tech. rep, US Geological Survey

D'Amato J, Hantz D, Guerin A et al (2016) Influence of meteorological factors on rockfall occurrence in a middle mountain limestone cliff. Nat Hazards Earth Syst Sci 16(3):719–735

De Biagi V, Napoli ML, Barbero M et al (2017) Estimation of the return period of rockfall blocks according to their size. Nat Hazards Earth Syst Sci 17(1):103–113

De Biagi V, Marchelli M, Peila D (2020) Reliability analysis and partial safety factors approach for rockfall protection structures. Eng Struct 213:110553

DESA U (2023) The sustainable development goals report 2023: special edition-July 2023. New York, USA

Dorren LK (2015) Rockyfor3d (v5. 2) revealed—transparent description of the complete 3d rockfall model. EcorisQ paper (www ecorisq org)

Farvacque M, Eckert N, Bourrier F et al (2021) Quantile-based individual risk measures for rockfall-prone areas. Int J Disaster Risk Reduction 53:101932
Gasser B (2022) Deathly accidents while high-altitude mountaineering in the swiss alps—an observational analysis from 2009 to 2021. Int J Environ Res Public Health 19(19):12498
Hantz D, Corominas J, Crosta GB et al (2021) Definitions and concepts for quantitative rockfall hazard and risk analysis. Geosciences 11(4):158
Hartmeyer I, Keuschnig M, Delleske R et al (2020) A 6-year lidar survey reveals enhanced rockwall retreat and modified rockfall magnitudes/frequencies in deglaciating cirques. Earth Surf Dynamics 8(3):753–768
Illeditsch M, Preh A (2024) Determination of meaningful block sizes for rockfall modelling. Nat Hazards 120(6):5685–5710
Jakob M (2022) Landslides in a changing climate. In: Landslide hazards, risks, and disasters. Elsevier, p 505–579
Knoflach B, Tussetschlaeger H, Sailer R et al (2021) High mountain rockfall dynamics: rockfall activity and runout assessment under the aspect of a changing cryosphere. Geogr Ann Series A Phys Geogr 103(1):83–102
Langenbach M, Jaccard E (2019) Innovation at the heart of tourism diversification in mountain resorts? A critical approach to the role of trail running in Switzerland. Mondes du tourisme (15). https://doi.org/10.4000/tourisme.1936, https://shs.hal.science/halshs-02353373
Lari S, Frattini P, Crosta G (2014) A probabilistic approach for landslide hazard analysis. Eng Geol 182:3–14
Li L, Lan H (2015) Probabilistic modeling of rockfall trajectories: a review. Bull Eng Geol Environ 74:1163–1176
Macciotta R, Martin CD, Cruden DM (2015) Probabilistic estimation of rockfall height and kinetic energy based on a three-dimensional trajectory model and Monte Carlo simulation. Landslides 12:757–772
Macciotta R, Hendry M, Cruden DM et al (2017) Quantifying rock fall probabilities and their temporal distribution associated with weather seasonality. Landslides 14(6):2025–2039
Mainieri R, Eckert N, Corona C et al (2023) Limited impacts of global warming on rockfall activity at low elevations: insights from two calcareous cliffs from the French Prealps. Prog Phys Geogr Earth Environ 47(1):50–73
Marchelli M, Biagi VD, Peila D (2020) Reliability-based design of protection net fences: influence of rockfall uncertainties through a statistical analysis. Geosciences 10(8):280
Marchelli M, De Biagi V, Peila D (2021) Reliability-based design of rockfall passive systems height. Int J Rock Mech Min Sci 139:104664
Marchelli M, De Biagi V, Bertolo D et al (2022) A mixed quantitative approach to evaluate rockfall risk and the maximum allowable traffic on road infrastructure. Georisk Assess Manag Risk Eng Syst Geohazards 16(3):584–594
McClung D (1999) The encounter probability for mountain slope hazards. Can Geotech J 36(6):1195–1196
Mirhadi N, Macciotta R (2023) Quantitative correlation between rock fall and weather seasonality to predict changes in rock fall hazard with climate change. Landslides 20:2227–2241
Moos C, Bontognali Z, Dorren L et al (2022) Estimating rockfall and block volume scenarios based on a straightforward rockfall frequency model. Eng Geol 309:106828
ONR 24810 (2021) Technical protection against rockfall - terms and definitions, effects of actions, design, monitoring and maintenance
Peila D, Ronco C (2009) Design of rockfall net fences and the new ETAG 027 European guideline. Nat Hazards Earth Syst Sci 9(4):1291–1298
Ravanel L, Deline P (2015) Rockfall hazard in the Mont Blanc massif increased by the current atmospheric warming. In: Engineering geology for society and territory-volume 1: climate change and engineering geology, Springer, pp 425–428
Rossi M, Sarro R, Reichenbach P et al (2021) Probabilistic identification of rockfall source areas at regional scale in El Hierro (Canary Islands, Spain). Geomorphology 381:107661
Ruiz-Carulla R, Corominas J, Mavrouli O (2017) A fractal fragmentation model for rockfalls. Landslides 14(3):875–889
Scavia C, Barbero M, Castelli M et al (2020) Evaluating rockfall risk: some critical aspects. Geosciences 10(3):98
Spadari M, Kardani M, De Carteret R et al (2013) Statistical evaluation of rockfall energy ranges for different geological settings of New South Wales, Australia. Eng Geol 158:57–65
Stoffel M, Trappmann DG, Coullie MI et al (2024) Rockfall from an increasingly unstable mountain slope driven by climate warming. Nat Geosci 17(3):249–254
UNI 11211-4 (2018) Opere di difesa dalla caduta massi - parte 4: Progetto definitivo ed esecutivo
Vagnon F, Bonetto S, Ferrero AM et al (2020) Eurocode 7 and rock engineering design: the case of rockfall protection barriers. Geosciences 10(8):305
Vigna S, Marchelli M, De Biagi V et al (2023) Numerical simulation of rockfall protection embankments in natural soil. Geosciences 13(12):368
Wang X, Frattini P, Crosta G et al (2014) Uncertainty assessment in quantitative rockfall risk assessment. Landslides 11:711–722

Maddalena Marchelli (✉)
Department of Environment, Land and Infrastructure Engineering, Politecnico di Torino, Corso Duca degli Abruzzi, 24, Torino 10129, Italy

Maddalena Marchelli
Email: maddalena.marchelli@polito.it

Valerio De Biagi · Bernardino Chiaia
Department of Structural, Geotechnical and Building Engineering, Politecnico di Torino, Corso Duca degli Abruzzi, 24, Torino 10129, Italy

Valerio De Biagi
Email: valerio.debiagi@polito.it

Bernardino Chiaia
Email: bernardino.chiaia@polito.it